frontiers | Frontiers in Materials

ORIGINAL RESEARCH
published: 11 April 2022
doi: 10.3389/fmats.2022.864478

A Cross-Linked Poly(Ethylene Oxide)-Based Electrolyte for All-Solid-State Lithium Metal Batteries With Long Cycling Stability

Chengzhou Xin, Kaihua Wen, Shundong Guan, Chuanjiao Xue, Xinbin Wu, Liangliang Li and Ce-Wen Nan**

State Key Laboratory of New Ceramics and Fine Processing, School of Materials Science and Engineering, Tsinghua University, Beijing, China

A cross-linked poly(ethylene oxide) (PEO)-based electrolyte with polyaryl polymethylene isocyanate (PAPI) as the cross-linking agent is synthesized by a facile one-pot reaction. The PEO chains are cross-linked by PAPI through the reaction between hydroxyl groups (–OH) and isocyanate groups (–N=C=O). The effects of PAPI on the electrochemical performance of the PEO-based electrolyte and the stability of the electrolyte/electrode interface are investigated. The PEO–PAPI electrolyte has an ionic conductivity of 9.3×10^{-5}–1.3×10^{-4} S cm^{-1} at 60°C. The cross-linked PEO–PAPI electrolyte exhibits enhanced mechanical properties compared to pristine PEO and shows good compatibility with a lithium (Li) metal anode. An all-solid-state Li metal battery (ASSLMB) with the optimized PEO–PAPI electrolyte and a $LiFePO_4$ cathode (1.62 mg cm^{-2} in mass loading) shows a discharge capacity of 112.8 mAh g^{-1} after 700 cycles with a current density of 88 μA cm^{-2} at 60°C. Even with a high mass loading of 8.4 mg cm^{-2}, the ASSLMB with the cross-linked PEO-based electrolyte shows a good cycle performance. The experimental data show that the cross-linked PEO–PAPI electrolyte is a promising candidate for solid electrolytes used in ASSLMBs.

Keywords: poly(ethylene oxide), polyaryl polymethylene isocyanate, solid electrolyte, solid-state battery, cross-linking

OPEN ACCESS

Edited by:
Howard Qingsong TU, Lawrence Berkeley National Laboratory, United States

Reviewed by:
Yang Zhao, Western University, Canada
Sébastien Maria, Aix-Marseille Université, France

****Correspondence:***
Liangliang Li
liliangliang@mail.tsinghua.edu.cn
Ce-Wen Nan
cwnan@mail.tsinghua.edu.cn

Specialty section:
This article was submitted to Energy Materials, a section of the journal Frontiers in Materials

Received: *28 January 2022*
Accepted: *16 March 2022*
Published: *11 April 2022*

Citation:
Xin C, Wen K, Guan S, Xue C, Wu X, Li L and Nan C-W (2022) A Cross-Linked Poly(Ethylene Oxide)-Based Electrolyte for All-Solid-State Lithium Metal Batteries With Long Cycling Stability. Front. Mater. 9:864478. doi: 10.3389/fmats.2022.864478

INTRODUCTION

All-solid-state lithium (Li) metal batteries (ASSLMBs) have drawn much attention because of their safety and high energy density. In ASSLMBs, flammable liquid electrolytes are replaced by non-flammable solid-state ones, and a Li metal anode with a high capacity is used (Du et al., 2015; Cheng et al., 2017; Liu et al., 2018; Lv et al., 2019; Xia et al., 2019). Various solid-state electrolytes with a high ionic conductivity, wide electrochemical stability window, and large Li-ion transference number have been developed (Bachman et al., 2016; Yang et al., 2017; Gao et al., 2018; Dirican et al., 2019; Jiang et al., 2020). Solid polymer electrolytes are more flexible and easily processible than inorganic electrolytes; therefore, they are suitable for commercial applications (Yue et al., 2016; Zhou et al., 2019). Many polymer electrolytes such as poly(ethylene oxide) (PEO), poly(vinylidene fluoride) (PVDF), poly(propylene carbonate) (PPC), and polyacrylonitrile (PAN) have been extensively studied (Han et al., 2015; Ben et al., 2016; Yue et al., 2016; Chen et al., 2018; Zhang et al., 2018; Lopez et al., 2019; Zhang et al., 2019). PEO, a well-known polymer electrolyte, has good stability against Li

metal, and the solubility of different Li salts in PEO is high. However, PEO has a low ionic conductivity, and it cannot inhibit Li dendrite growth due to poor mechanical properties (Bao et al., 2018).

PEO's ionic conductivity depends on segmental motion in the amorphous region of the polymer (Lopez et al., 2019). Various methods such as cross-linking, polymer blending, and adding nano-fillers and additives have been used to increase the proportion of the amorphous phase in PEO in order to raise PEO's ionic conductivity (Chen et al., 2016a; Li et al., 2018; Wang et al., 2018; Zhu et al., 2018; Falco et al., 2019). In addition to the ionic conductivity enhancement, cross-linking can also improve the mechanical properties of PEO or poly(ethylene glycol) (PEG), which is beneficial for the cycling stability of PEO-based solid-state batteries (Chen et al., 2016b; Lan et al., 2017). Ultraviolet (UV) photocuring and thermal polymerization are often used to synthesize cross-linking PEO/PEG to enhance the electrochemical performance (Malucellia et al., 2005; Pan et al., 2015; Porcarelli et al., 2016; Falco et al., 2019). Falco et al. synthesized a UV-cross-linked polymer electrolyte based on PEO, tetra(ethylene glycol)dimethyl ether, and lithium bis-(trifluoromethane)sulfonamide (LiTFSI) and proved that UV-induced cross-linking was an effective method to reduce the electrolyte's crystallinity and improve the Li^+ transport number and ionic conductivity (Falco et al., 2019). Pan et al. reported a solid polymer electrolyte with octakis(3-glycidyloxypropyldimethylsiloxy)octasilsesquioxane as the cross-linker, amine-terminated PEG as the polymer, and LiTFSI as the Li salt. The polymer electrolyte with enhanced mechanical properties prohibited the growth of Li dendrites (Pan et al., 2015). Chen et al. designed a copolymer electrolyte by cross-linking trimethylolpropane triglycidyl ether with poly(ethylene glycol) diamine, which showed high ionic conductivity and rendered a stable cycle performance to $LiFePO_4$-based batteries (Chen et al., 2016b).

In addition to the ionic conductivity and mechanical properties of PEO, the interfacial compatibility between the electrolyte and a Li metal anode is also important for the battery's cycle performance (Dai et al., 2018). It is necessary to achieve uniform Li deposition on Li anodes because uneven Li deposition causes the growth of Li dendrites, formation of dead Li, and even the short circuit of batteries (Lu et al., 2017; Chai et al., 2018; Duan et al., 2018; Wu et al., 2018). Khurana et al. designed a cross-linked polyethylene/PEO polymer electrolyte and found that the tortuous nanoporous network in the electrolyte may limit the growth of micrometer-sized Li dendrites (Khurana et al., 2014).

However, the cycle performance of most ASSLMBs with cross-linked PEO is not satisfactory, and the mass loading of active materials in composite cathodes is usually low, limiting the cell's energy density (Yang et al., 2019). In this work, we synthesize a cost-effective cross-linked PEO-based electrolyte with polyaryl polymethylene isocyanate (PAPI) by a one-pot reaction. The cross-linking network structure of PEO chain segments is acquired through the reaction between the hydroxyl groups (−OH) in PEO and multiple isocyanate groups (−N=C=O) in PAPI. The cross-linked PEO-based electrolyte shows better film-forming ability and mechanical properties than a pristine PEO electrolyte. Based on the cross-linked PEO, an ASSLMB with an active material mass loading of 1.62 mg cm^{-2} shows a stable long-term cycle performance of up to 700 cycles. Even with a high mass loading of 8.4 mg cm^{-2}, the ASSLMB can steadily run for 180 cycles. Our work shows that the cross-linked PEO–PAPI electrolyte is a promising candidate for solid electrolytes used in ASSLMBs.

EXPERIMENTAL SECTION

PEO (M_w ~600,000, Sigma-Aldrich) and LiTFSI (Sigma-Aldrich) with a weight ratio of 3:1 were mixed and dissolved into acetonitrile (ACN). In a typical experiment, the total weight of PEO plus LiTFSI was 0.8 g, and the volume of ACN was 8 ml. PAPI (M_w 380–400, ~23 wt. % in chlorobenzene) was purchased from Liaoning Hongshan Chemical Co. Ltd. PAPI solution with a volume of 0, 0.1, 0.2, 0.3, or 0.4 ml was added to the PEO–LiTFSI–ACN solution. Then, the mixture was stirred for more than 12 h to obtain a homogenous solution. Next, the solution was cast onto a poly(tetrafluoroethylene) substrate and kept at 70°C for at least 12 h to accomplish the cross-linking reaction between PEO and PAPI and remove the solvent. The resulting PEO–PAPI electrolyte membrane with a thickness of ~140–180 μm was peeled off from the substrate and stored in an argon (Ar)-filled glove box (O_2 < 0.1 ppm, H_2O < 0.1 ppm).

Scanning electron microscopy (SEM, Zeiss Merlin) was performed to analyze the morphology of PEO-based electrolyte membranes and Li metal electrodes. X-ray diffractometry (XRD, Rigaku D/max-2500 with Cu-Kα, 40 kV and 200 mA) and Fourier transform infrared spectroscopy (FTIR, Bruker Tensor 27 spectrometer) were performed to analyze the phase structure and chemical groups of the PEO-based electrolytes, respectively. Thermogravimetric analysis–differential scanning calorimetry (TGA/DSC, METTLER TOLEDO 1 HT/1,600) in an Ar atmosphere was performed to study the thermal stability of the electrolytes. A differential scanning calorimeter (DSC Q2000, TA Instruments) was used to measure the glass transition temperature T_g of the electrolytes. X-ray photoelectron spectroscopy (XPS, PHI Quantera II) was used to study the electrolyte/electrode interface after cycling. The stretching test of the electrolyte with a size of ~10 mm × 17 mm × 0.15 mm was performed using a Shimadzu EZ-LX HS machine with a stretching speed of 30 mm min^{-1}.

A stainless steel (SS)||PEO-based electrolyte||SS coin cell was assembled to measure the ionic conductivity of the electrolyte by using an impedance analyzer (ZAHNER-elecktrik IM6) at 25–120°C at a frequency range of 0.1 Hz–8 MHz. A Li||PEO-based electrolyte||SS coin cell was used to test the electrochemical stability window of the electrolyte by linear sweep voltammetry (LSV, Bio-Logic VMP3) with a rate of 0.1 mV s^{-1}. A Li||PEO-based electrolyte||Li symmetric cell was used to investigate the stability of the electrolyte against Li metal. CR2025 coin-type ASSLMBs were assembled with a $LiFePO_4$ or

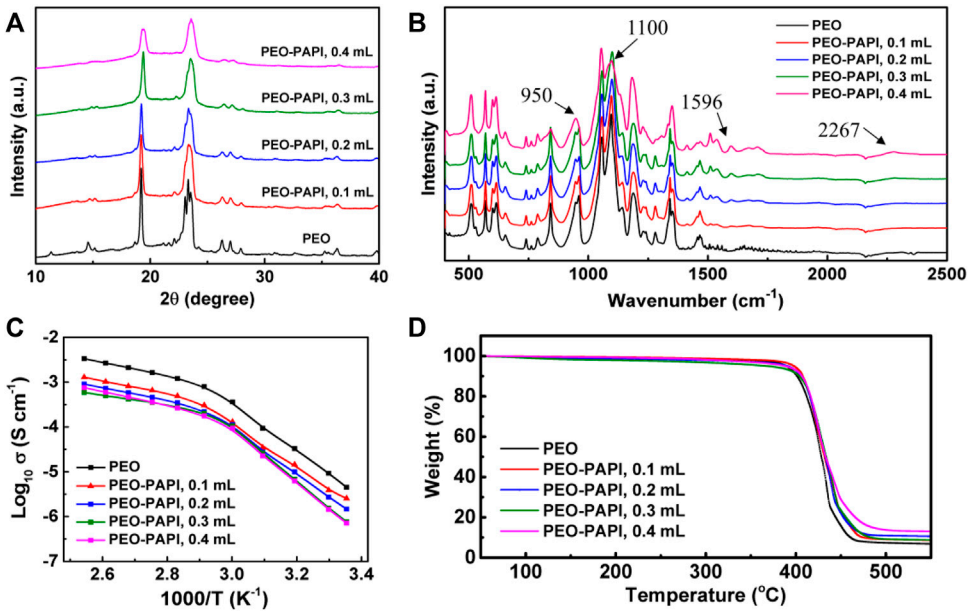

FIGURE 1 | (A) XRD patterns, **(B)** FTIR spectra, **(C)** Arrhenius plots of ionic conductivity, and **(D)** TGA curves of the PEO–PAPI electrolytes. The volumes of PAPI used in the electrolyte preparation were 0, 0.1, 0.2, 0.3, and 0.4 ml. In **(B)**, the peaks at 950, 1,100, 1,596, and 2,267 cm^{-1} are assigned to the CH_2 rocking vibration, C-O-C stretching vibration, phenyl group, and –N=C=O group, respectively.

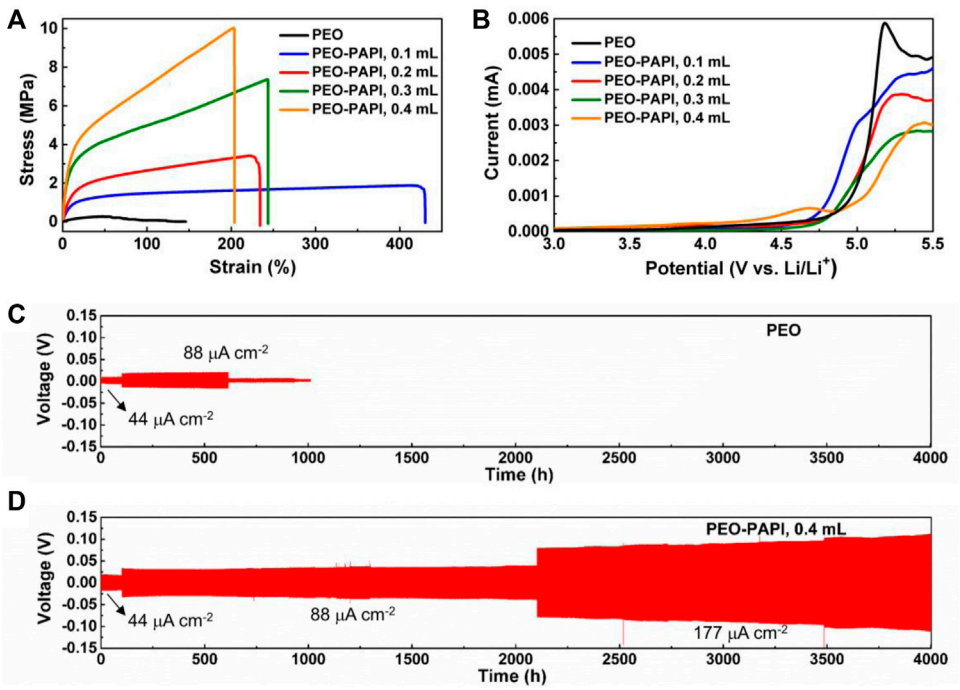

FIGURE 2 | (A) Stress–stain curves and **(B)** LSV curves of the PEO–PAPI electrolytes. **(C)** Cycle performance of a Li symmetric cell with a pristine PEO electrolyte at 60°C. **(D)** Cycle performance of a Li symmetric cell with a PEO–PAPI (0.4 ml) electrolyte at 60°C. The applied current density in **(C)** and **(D)** increases from 44 to 88 and 177 μA cm^{-2}, and the corresponding durations are 101, 2000, and 1900 h, respectively.

$LiNi_{0.6}Co_{0.2}Mn_{0.2}O_2$ (NCM) composite cathode, PEO-based electrolyte membrane, and Li metal anode. The composite cathode contains $LiFePO_4$ or NCM, super-P carbon black (TeenSky Inc.), PEO, and LiTFSI with a weight ratio of 8:1:1:0.5. The cycle performance of the ASSLMBs was measured using a battery test system (CT 2001A, LANHE, China) at 60°C. The

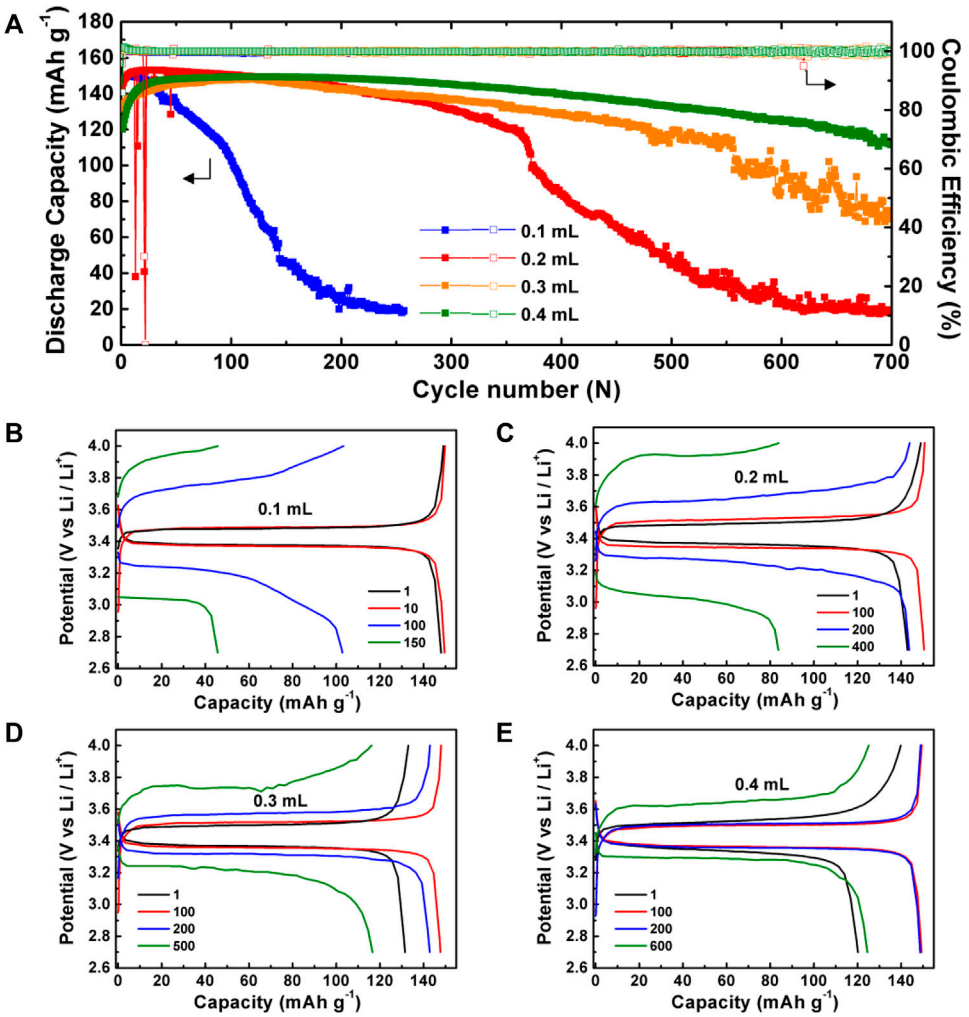

FIGURE 3 | (A) Cycle performance of $LiFePO_4$||PEO–PAPI electrolyte||Li ASSLMBs at 60°C. **(B–E)** Charge–discharge curves with different cycle numbers of the ASSLMBs with the PEO–PAPI electrolytes. The volumes of PAPI in **(B–E)** were 0.1, 0.2, 0.3, and 0.4 ml, respectively.

voltage ranges for a $LiFePO_4$ battery and an NCM battery were 2.7–4.0 and 3.0–4.2 V, respectively.

RESULTS AND DISCUSSION

Figure 1A shows the XRD patterns of PEO–PAPI electrolytes with 0–0.4 ml PAPI. All the five samples show crystalline peaks at ~ 19° and 23.5°, indicating that the crystal structure of PEO remains after PAPI is added (Wang et al., 2018). It can be observed that the peaks at 23.5° of the electrolytes with PAPI become broader in comparison with those of the pure PEO sample, indicating the reduction of the crystallinity of the PEO–PAPI electrolytes due to cross-linking (Falco et al., 2019). **Figure 1B** presents the FTIR spectra of the PEO electrolytes with and without PAPI. The peak at 1,596 cm^{-1} is assigned to the phenyl group of PAPI (Chen et al., 2017). The absorption peak of –N=C=O groups at ~ 2,267 cm^{-1} disappears in the electrolytes with 0.1 or 0.2 ml PAPI due to the cross-linking reaction between the –N=C=O groups of PAPI and the hydroxyl end groups (–OH group) of PEO (Gong et al., 2016; Zeng et al., 2018), whereas it appears in the sample with 0.4 ml PAPI, indicating the excess of PAPI. In addition, the peaks at ~ 950 and 1,100 cm^{-1} are assigned to the CH_2 rocking vibration and C-O-C stretching vibration in PEO, respectively (Chen et al., 2016b; Anilkumar et al., 2017).

The Arrhenius plots of ionic conductivity σ of the PEO–PAPI electrolytes are shown in **Figure 1C**. For all the samples, the ionic conductivity increases continuously from room temperature (RT) to 120°C. At ~ 60°C, the slopes of the Arrhenius plots change because of the formation of the amorphous phase from the PEO crystals (Chen et al., 2016a; Wang et al., 2018). When the cross-linking agent PAPI is added to PEO, the ionic conductivity decreases. **Supplementary Figure S1** (Supplementary Material) shows that the T_g of the electrolyte slightly increases after PAPI is

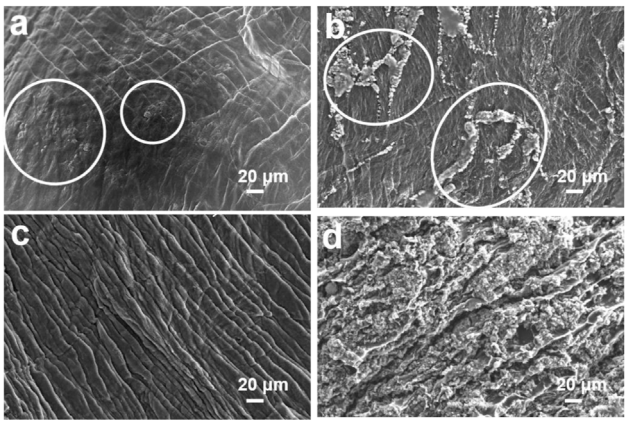

FIGURE 4 | SEM images of the Li anode surfaces in the ASSLMBs with a pristine PEO electrolyte membrane after **(A)** three cycles and **(B)** 101 cycles. SEM images of the Li anode surfaces in the ASSLMBs with a PEO–PAPI (0.4 ml) electrolyte membrane after **(C)** six cycles and **(D)** 101 cycles. Li dendrites in **(A)** and **(B)** are marked by white circles.

added, indicating the reduction of the local segmental mobility of PEO chains (Bao et al., 2018; Falco et al., 2019). Therefore, the ionic conductivity of the electrolyte with PAPI is reduced. With PAPI, the ionic conductivity values at 60 and 120°C are in the ranges of 9.3×10^{-5}–1.3×10^{-4} and 5.9×10^{-4}–1.3×10^{-3} S cm^{-1}, respectively, meaning that the cross-linked PEO-based electrolyte may be operated at a temperature of 60°C and more.

The thermal stability of the PEO–PAPI electrolytes was evaluated by TGA, and the results are summarized in **Figure 1D**. The cross-linked PEO–PAPI electrolytes show almost no weight loss from RT to 200°C, indicating that there is no residual solvent in the electrolytes. All these electrolytes are stable up to 400°C, indicating that PAPI does not degrade the thermal stability of PEO. A large weight loss occurs at ~ 400°C due to the decomposition of PEO.

Supplementary Figures S2A–D (Supplementary Material) show the photographs of the PEO–PAPI electrolyte membranes with different PAPI contents. The film-forming ability of the cross-linked electrolytes is much better than that of the PEO electrolyte without PAPI (**Supplementary Figure S3**, Supplementary Material). For the cases of 0.1–0.3 ml PAPI, the membranes are homogeneous (**Supplementary Figures S2A–C**), whereas the surface of the electrolyte with 0.4 ml PAPI is not uniform (**Supplementary Figure S2D**). The SEM images in **Supplementary Figures S2E–H** show that all the PEO–PAPI electrolyte membranes are dense. The one with 0.4 ml PAPI has some particle-like agglomeration due to excessive PAPI (**Supplementary Figure S2H**). The mechanical properties of the PEO–PAPI electrolytes were characterized by the tensile test. The stress–strain curves of the electrolytes are compared in **Figure 2A**. The maximum stress value in the curve is used to evaluate the tensile strength. With the increase of PAPI, the tensile strength continuously increases. The tensile strength of the PEO–PAPI membrane with 0.4 ml PAPI reaches 10.0 MPa, which is much higher than that of the membrane without PAPI. The values of Young's

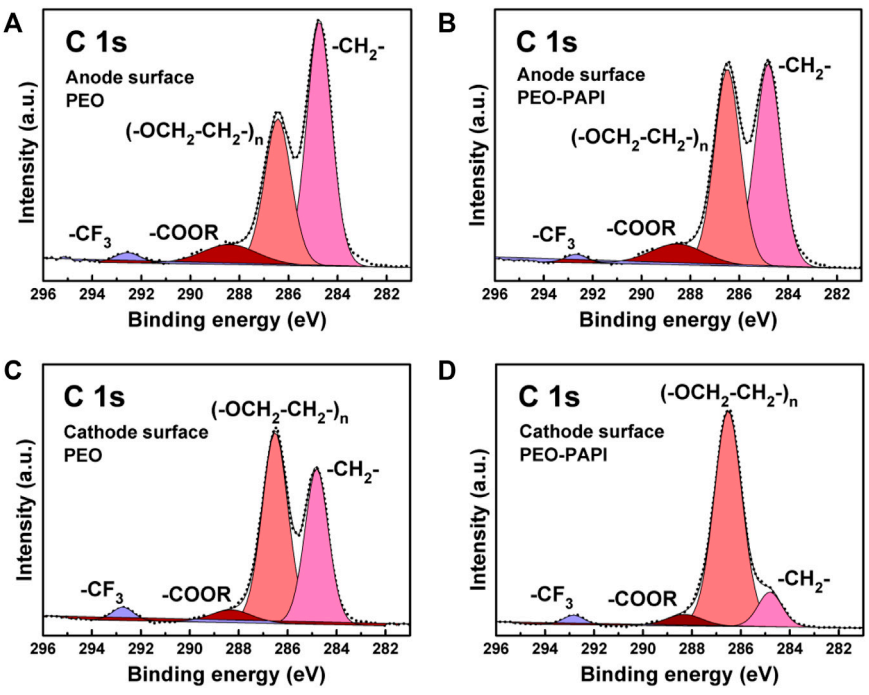

FIGURE 5 | XPS C 1s spectra on the Li anodes of the ASSLMBs with **(A)** pristine PEO and **(B)** PEO–PAPI (0.4 ml) membranes after cycling. XPS C 1s spectra on the cathodes of the ASSLMBs with **(C)** pristine PEO and **(D)** PEO–PAPI (0.4 ml) membranes after cycling.

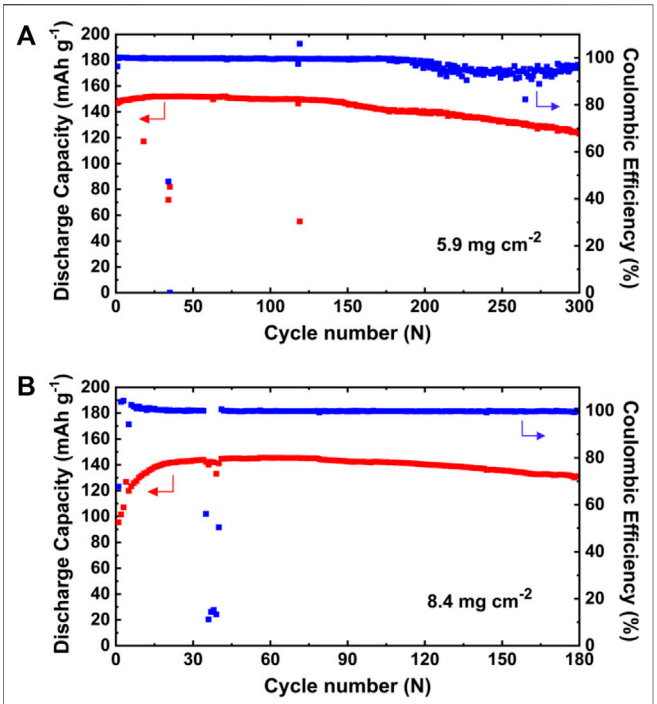

FIGURE 6 | Cycle performance of $LiFePO_4$||PEO–PAPI (0.4 ml) electrolyte||Li ASSLMBs with a high mass loading of $LiFePO_4$ at 60°C. **(A)** 5.9 and **(B)** 8.4 mg cm^{-2}.

modulus are 1.6, 11.7, 18.0, 43.7, and 49.4 MPa in the PEO-based electrolytes with 0, 0.1, 0.2, 0.3, and 0.4 ml PAPI, respectively. Such significantly enhanced tensile strengths and Young's modulus are beneficial for the cycle performance of batteries.

The electrochemical stability of the PEO–PAPI electrolytes was studied by LSV measurement at RT. In **Figure 2B**, it can be observed that the electrochemical stability window is ~4.5 V for the electrolytes with 0–0.3 ml PAPI and is ~4.0 V for the one with 0.4 ml PAPI. The addition of PAPI decreases the electrochemical stability window of the electrolyte, possibly due to the low oxidation potential of PAPI (Wang et al., 2015). All the PEO–PAPI electrolytes are stable up to 4.0 V; therefore, they are suitable for $LiFePO_4$-based Li-ion batteries.

Next, Li||PEO-based electrolyte||Li symmetric cells were assembled to evaluate the interfacial stability between the electrolytes and Li metal electrodes. In the cycling test, the symmetric cells were periodically charged and discharged for 0.5 h at 60°C. The applied current density increased from 44 to 88 and 177 μA cm^{-2}, and the corresponding durations are 101, 2000, and 1900 h, respectively (**Figures 2C, D**). For the cell based on the electrolyte without PAPI, short circuit occurs at 88 μA cm^{-2} after 615 h of cycling (**Figure 2C**). In contrast, the cell with a PEO–PAPI (0.4 ml) electrolyte membrane shows a highly stable cycle performance for 4,001 h with elevated current densities (**Figure 2D**). The electrolyte with enhanced tensile strength and Young's modulus by the cross-linking reaction between PEO and PAPI successfully inhibits the growth of Li dendrites and avoids the occurrence of short circuit.

Based on the results of the electrochemical stability window in **Figure 2B**, $LiFePO_4$||PEO–PAPI electrolyte||Li ASSLMBs were assembled and tested at 88 μA cm^{-2} at 60 C. The mass loading of $LiFePO_4$ was 1.62 ± 0.07 mg cm^{-2}. **Figure 3** shows the cycle performance and corresponding charge–discharge curves of the ASSLMBs with various PEO–PAPI electrolyte membranes. For comparison, the charge–discharge curves of the ASSLMB with a pristine PEO electrolyte are shown in **Supplementary Figure S4** (Supplementary Material). Without PAPI, the cell's capacity rapidly drops just after three cycles. With PAPI, the cycle life of the ASSLMB is significantly extended (**Figure 3A**). The more the PAPI content is, the better the cycle performance of the ASSLMB will be. For the case of 0.4 ml PAPI, the ASSLMB lasts for 700 cycles and delivers a final discharge capacity of 112.8 mAh g^{-1}. This PEO–PAPI (0.4 ml) electrolyte membrane with the largest tensile strength and Young's modulus (**Figure 2A**) has the highest ability to inhibit the growth of Li dendrites; therefore, it renders the best cycle performance to the ASSLMB.

Some ASSLMBs with pristine PEO and PEO–PAPI (0.4 ml) electrolyte membranes were dissembled after cycling with a current density of 88 μAcm^{-2} at 60°C, and the surfaces of the Li anodes were observed by SEM. For a cell with a pristine PEO membrane, uneven Li deposition was observed on the Li anode for just three cycles (**Figure 4A**). For another cell with pristine PEO, the discharge capacity suddenly dropped to ~14 mAh g^{-1} after six cycles due to the growth of Li dendrites, generation of dead Li, and even occurrence of a micro-short circuit. Then, obvious Li dendrites were seen on this cell's anode surface after 101 cycles (**Figure 4B**). These phenomena are similar to those in other works (Bao et al., 2018; Zou et al., 2018). In contrast, the Li deposition on the anodes of the cells with a PEO–PAPI (0.4 ml) membrane is much more uniform. For a cell with the PEO–PAPI membrane after six cycles, the surface of the Li anode is as fresh as that of a pristine Li foil (**Figure 4C**). For another cell with the PEO–PAPI membrane after 101 cycles, the Li deposition is still uniform on the anode (**Figure 4D**); therefore, the discharge capacity remains at 150.4 mAh g^{-1}. The SEM images in **Figure 4** confirm that the PEO–PAPI (0.4 ml) electrolyte has an excellent ability of suppressing Li dendrites.

Next, XPS was carried out to study the chemical components on the surfaces of the anodes and cathodes of the ASSLMBs after cycling. In the XPS tests, a battery with a PEO–PAPI (0.4 ml) membrane was analyzed after 217 cycles (the discharge capacity was 125.9 mAh g^{-1}), and a cycled battery with a pristine PEO membrane was dissembled after failure (the discharge capacity dropped to ~0 mAh g^{-1}). **Figure 5A** and **Figure 5B** show the XPS C 1s spectra on the Li anode surfaces for the cases of pristine PEO and PEO–PAPI membranes, respectively. The $(-OCH_2-CH_2-)_n$ peak at ~ 286.6 eV represents PEO, and the –COOR peak at ~ 288.4 eV is attributed to the decomposition product of PEO (Simon et al., 2020). The–COOR to $(-OCH_2-CH_2-)_n$ peak intensity ratio is smaller for the case of PEO–PAPI, indicating less decomposition of the PEO–PAPI electrolyte during cycling. The XPS C 1s spectra on the cathode surfaces for

the ASSLMBs with pristine PEO and PEO–PAPI show the same result in terms of the –COOR to $(–OCH_2–CH_2–)_n$ peak intensity ratio (**Figures 5C, D**). Thus, the cross-linking network structure in the PEO–PAPI membrane reduces the decomposition of the electrolyte in the charge/discharge processes due to the enhanced tensile strength and Young's modulus. In addition, the XPS F 1s and S 2p spectra on the anodes (**Supplementary Figure S5**, Supplementary Material) and cathodes (**Supplementary Figure S6**, Supplementary Material) exhibit the $–CF_3$ and $–SO_2CF_3$ peaks representing LiTFSI and the LiF, respectively, and $–SO_2CF_2^+$/$Li_xS_yO_z$ peaks originated from the decomposition of LiTFSI (Simon et al., 2020). On the cathode, the LiF to $–CF_3$ peak intensity ratio for PEO–PAPI is smaller than that for pristine PEO, and the $–SO_2CF_2^+$ peak cannot be detected for PEO–PAPI, indicating that the PEO–PAPI membrane is more stable than the pristine PEO one when the applied voltage is ≤4.0 V.

Next, the $LiFePO_4$||PEO–PAPI (0.4 ml) electrolyte||Li ASSLMBs with a high mass loading of active material were prepared, and their cycle performance at 88 μA cm^{-2} and 60°C is shown in **Figure 6**. The mass loadings of $LiFePO_4$ in the cathodes are 5.9 and 8.4 mg cm^{-2}, as shown in **Figures 6A, B**, respectively. These batteries also have a long cycle life (300 and 180 cycles for the cases of 5.9 and 8.4 mg cm^{-2}, respectively). In addition, a $LiNi_{0.6}Co_{0.2}Mn_{0.2}O_2$ (NCM)||PEO–PAPI (0.4 ml) electrolyte||Li battery was assembled and cycled for 110 cycles between 3.0 and 4.2 V at 60°C (**Supplementary Figure S7**, Supplementary material). The electrolytes with a PAPI content of ≤0.3 ml have a wider electrochemical stability window, but their tensile strength and Young's modulus are lower. Thus, the electrolyte with 0.4 ml PAPI was used in the NCM||Li battery in this work. The cycle life of the NCM-based battery could be prolonged by optimizing both the electrochemical stability window and mechanical properties of the PEO–PAPI electrolytes, which will be our future work. All the experimental results show that the PEO–PAPI electrolyte has good potential in the Li metal batteries with a high-mass-loading or high-voltage cathode.

CONCLUSION

The cross-linking agent PAPI is introduced to PEO to prepare a cross-linked PEO–PAPI electrolyte through a one-pot reaction. The PEO–PAPI electrolytes prepared with various amounts of PAPI have an ionic conductivity of 9.3×10^{-5}–1.3×10^{-4} S cm^{-1} at 60°C and possess enhanced mechanical properties and better interfacial stability with Li metal compared with the pristine PEO electrolyte without PAPI. The ASSLMB with the optimized PEO–PAPI electrolyte and a $LiFePO_4$ cathode shows a long cycle life of 700 cycles at 60°C. Even with a high $LiFePO_4$ mass loading of 8.4 mg cm^{-2}, the ASSLMB based on the PEO–PAPI electrolyte also shows a stable cycle performance. Due to the cross-linking network structure, the decomposition of the cross-linked PEO–PAPI electrolyte is less than that of a pristine PEO one during charge/discharge cycling. The experimental data show that the cycle performance of the ASSLMBs with the PEO–PAPI electrolyte is affected by the mechanical properties of the cross-linked solid electrolyte, and the cost-effective cross-linked PEO-based electrolyte with PAPI is a promising candidate for solid electrolytes used in ASSLMBs.

DATA AVAILABILITY STATEMENT

The original contributions presented in the study are included in the article/**Supplementary Material**, further inquiries can be directed to the corresponding authors.

AUTHOR CONTRIBUTIONS

CXi was responsible for conducting experiments, data analysis, and manuscript writing. KW, SG, CXu and XW were responsible for data analysis. LL and C-WN were responsible for experimental design and manuscript revision.

FUNDING

This work was supported by the National Natural Science Foundation of China under Grant Nos. 51788104 and U21A2080.

SUPPLEMENTARY MATERIAL

The Supplementary Material for this article can be found online at: https://www.frontiersin.org/articles/10.3389/fmats.2022.864478/full#supplementary-material

REFERENCES

Anilkumar, K. M., Jinisha, B., Manoj, M., and Jayalekshmi, S. (2017). Poly(ethylene Oxide) (PEO) - Poly(vinyl Pyrrolidone) (PVP) Blend Polymer Based Solid Electrolyte Membranes for Developing Solid State Magnesium Ion Cells. *Eur. Polym. J.* 89, 249–262. doi:10.1016/j.eurpolymj.2017.02.004

Bachman, J. C., Muy, S., Grimaud, A., Chang, H.-H., Pour, N., Lux, S. F., et al. (2016). Inorganic Solid-State Electrolytes for Lithium Batteries: Mechanisms and Properties Governing Ion Conduction. *Chem. Rev.* 116, 140–162. doi:10.1021/acs.chemrev.5b00563

Bao, J., Qu, X., Qi, G., Huang, Q., Wu, S., Tao, C., et al. (2018). Solid Electrolyte Based on Waterborne Polyurethane and Poly(ethylene Oxide) Blend Polymer for All-Solid-State Lithium Ion Batteries. *Solid State Ionics* 320, 55–63. doi:10.1016/j.ssi.2018.02.030

Ben youcef, H., Garcia-Calvo, O., Lago, N., Devaraj, S., and Armand, M. (2016). Cross-Linked Solid Polymer Electrolyte for All-Solid-State Rechargeable Lithium Batteries. *Electrochim. Acta* 220, 587–594. doi:10.1016/j.electacta.2016.10.122

Chai, J., Chen, B., Xian, F., Wang, P., Du, H., Zhang, J., et al. (2018). Dendrite-Free Lithium Deposition via Flexible-Rigid Coupling Composite Network for $LiNi_{0.5}Mn_{1.5}O_4$/Li Metal Batteries. *Small* 14, 1802244. doi:10.1002/smll.201802244

Chen, B., Huang, Z., Chen, X., Zhao, Y., Xu, Q., Long, P., et al. (2016a). A New Composite Solid Electrolyte PEO/Li10GeP2S12/SN for All-Solid-State Lithium Battery. *Electrochim. Acta* 210, 905–914. doi:10.1016/j.electacta.2016.06.025

Chen, B., Xu, Q., Huang, Z., Zhao, Y., Chen, S., and Xu, X. (2016b). One-Pot Preparation of New Copolymer Electrolytes with Tunable Network Structure for All-Solid-State Lithium Battery. *J. Power Sourc.* 331, 322–331. doi:10.1016/j.jpowsour.2016.09.063

Chen, F., Zha, W., Yang, D., Cao, S., Shen, Q., Zhang, L., et al. (2018). All-Solid-State Lithium Battery Fitted with Polymer Electrolyte Enhanced by Solid Plasticizer and Conductive Ceramic Filler. *J. Electrochem. Soc.* 165, A3558–A3565. doi:10.1149/2.1371814jes

Chen, L., Zhang, S., Chen, Y., and Jian, X. (2017). Low Vanadium Ion Permeabilities of Sulfonated Poly(phthalazinone Ether Ketone)s Provide High Efficiency and Stability for Vanadium Redox Flow Batteries. *J. Power Sourc.* 355, 23–30. doi:10.1016/j.jpowsour.2017.04.045

Cheng, S. H.-S., He, K.-Q., Liu, Y., Zha, J.-W., Kamruzzaman, M., Ma, R. L.-W., et al. (2017). Electrochemical Performance of All-Solid-State Lithium Batteries Using Inorganic Lithium Garnets Particulate Reinforced PEO/LiClO4 Electrolyte. *Electrochimica Acta* 253, 430–438. doi:10.1016/j.electacta.2017.08.162

Dai, J., Yang, C., Wang, C., Pastel, G., and Hu, L. (2018). Interface Engineering for Garnet-Based Solid-State Lithium-Metal Batteries: Materials, Structures, and Characterization. *Adv. Mater.* 30, 1802068. doi:10.1002/adma.201802068

Dirican, M., Yan, C., Zhu, P., and Zhang, X. (2019). Composite Solid Electrolytes for All-Solid-State Lithium Batteries. *Mater. Sci. Eng. R: Rep.* 136, 27–46. doi:10.1016/j.mser.2018.10.004

Du, F., Zhao, N., Li, Y., Chen, C., Liu, Z., and Guo, X. (2015). All Solid State Lithium Batteries Based on Lamellar Garnet-type Ceramic Electrolytes. *J. Power Sourc.* 300, 24–28. doi:10.1016/j.jpowsour.2015.09.061

Duan, H., Yin, Y.-X., Shi, Y., Wang, P.-F., Zhang, X.-D., Yang, C.-P., et al. (2018). Dendrite-Free Li-Metal Battery Enabled by a Thin Asymmetric Solid Electrolyte with Engineered Layers. *J. Am. Chem. Soc.* 140, 82–85. doi:10.1021/jacs.7b10864

Falco, M., Simari, C., Ferrara, C., Nair, J. R., Meligrana, G., Bella, F., et al. (2019). Understanding the Effect of UV-Induced Cross-Linking on the Physicochemical Properties of Highly Performing PEO/LiTFSI-Based Polymer Electrolytes. *Langmuir* 35, 8210–8219. doi:10.1021/acs.langmuir.9b00041

Gao, Z., Sun, H., Fu, L., Ye, F., Zhang, Y., Luo, W., et al. (2018). Promises, Challenges, and Recent Progress of Inorganic Solid-State Electrolytes for All-Solid-State Lithium Batteries. *Adv. Mater.* 30, 1705702. doi:10.1002/adma.201705702

Gong, X., Shi, D., Zeng, H., Yang, Y., Jiang, T., Zhang, Q., et al. (2016). Facile One Pot Polycondensation Method to Synthesize the Crosslinked Polyethylene Glycol-Based Copolymer Electrolytes. *Macromol. Chem. Phys.* 217, 1607–1613. doi:10.1002/macp.201600040

Han, P., Zhu, Y., and Liu, J. (2015). An All-Solid-State Lithium Ion Battery Electrolyte Membrane Fabricated by Hot-Pressing Method. *J. Power Sourc.* 284, 459–465. doi:10.1016/j.jpowsour.2015.03.058

Jiang, T., He, P., Wang, G., Shen, Y., Nan, C. W., and Fan, L. Z. (2020). Solvent-Free Synthesis of Thin, Flexible, Nonflammable Garnet-Based Composite Solid Electrolyte for All-Solid-State Lithium Batteries. *Adv. Energ. Mater.* 10, 1903376. doi:10.1002/aenm.201903376

Khurana, R., Schaefer, J. L., Archer, L. A., and Coates, G. W. (2014). Suppression of Lithium Dendrite Growth Using Cross-Linked Polyethylene/Poly(ethylene Oxide) Electrolytes: A New Approach for Practical Lithium-Metal Polymer Batteries. *J. Am. Chem. Soc.* 136, 7395–7402. doi:10.1021/ja502133j

Lan, Q., Tang, S., Liang, J., Cheng, Q., Liu, C., Zhao, J., et al. (2017). Preparation and Characterization of Super Cross-Linked Poly(ethylene Oxide) Gel Polymer Electrolyte for Lithium-Ion Battery. *Sci. Adv. Mater.* 9, 988–994. doi:10.1166/sam.2017.3086

Li, Y.-J., Fan, C.-Y., Zhang, J.-P., and Wu, X.-L. (2018). A Promising PMHS/PEO Blend Polymer Electrolyte for All-Solid-State Lithium Ion Batteries. *Dalton Trans.* 47, 14932–14937. doi:10.1039/c8dt02904k

Liu, Q., Geng, Z., Han, C., Fu, Y., Li, S., He, Y.-b., et al. (2018). Challenges and Perspectives of Garnet Solid Electrolytes for All Solid-State Lithium Batteries. *J. Power Sourc.* 389, 120–134. doi:10.1016/j.jpowsour.2018.04.019

Lopez, J., Mackanic, D. G., Cui, Y., and Bao, Z. (2019). Designing Polymers for Advanced Battery Chemistries. *Nat. Rev. Mater.* 4, 312–330. doi:10.1038/s41578-019-0103-6

Lu, Q., He, Y.-B., Yu, Q., Li, B., Kaneti, Y. V., Yao, Y., et al. (2017). Dendrite-Free, High-Rate, Long-Life Lithium Metal Batteries with a 3D Cross-Linked Network Polymer Electrolyte. *Adv. Mater.* 29, 1604460. doi:10.1002/adma.201604460

Lv, F., Wang, Z., Shi, L., Zhu, J., Edström, K., Mindemark, J., et al. (2019). Challenges and Development of Composite Solid-State Electrolytes for High-Performance Lithium Ion Batteries. *J. Power Sourc.* 441, 227175. doi:10.1016/j.jpowsour.2019.227175

Malucellia, G., Priola, A., Sangermano, M., Amerio, E., Zini, E., and Fabbric, E. (2005). Hybrid Nanocomposites Containing Silica and PEO Segments: Preparation through Dual-Curing Process and Characterization. *Polymer* 46, 2872–2879. doi:10.1016/j.polymer.2005.02.045

Pan, Q., Smith, D. M., Qi, H., Wang, S., and Li, C. Y. (2015). Hybrid Electrolytes with Controlled Network Structures for Lithium Metal Batteries. *Adv. Mater.* 27, 5995–6001. doi:10.1002/adma.201502059

Porcarelli, L., Gerbaldi, C., Bella, F., and Nair, J. R. (2016). Super Soft All-Ethylene Oxide Polymer Electrolyte for Safe All-Solid Lithium Batteries. *Sci. Rep.* 6, 19892. doi:10.1038/srep19892

Simon, F. J., Hanauer, M., Richter, F. H., and Janek, J. (2020). Interphase Formation of PEO20:LiTFSI-Li6PS5Cl Composite Electrolytes with Lithium Metal. *ACS Appl. Mater. Inter.* 12, 11713–11723. doi:10.1021/acsami.9b22968

Wang, R., Li, X., Wang, Z., Guo, H., and Wang, J. (2015). Electrochemical Analysis for Cycle Performance and Capacity Fading of Lithium Manganese Oxide Spinel Cathode at Elevated Temperature Using P-Toluenesulfonyl Isocyanate as Electrolyte Additive. *Electrochimica Acta* 180, 815–823. doi:10.1016/j.electacta.2015.09.019

Wang, X., Zhang, Y., Zhang, X., Liu, T., Lin, Y.-H., Li, L., et al. (2018). Lithium-Salt-Rich PEO/Li0.3La0.557TiO3 Interpenetrating Composite Electrolyte with Three-Dimensional Ceramic Nano-Backbone for All-Solid-State Lithium-Ion Batteries. *ACS Appl. Mater. Inter.* 10, 24791–24798. doi:10.1021/acsami.8b06658

Wu, B., Wang, S., Lochala, J., Desrochers, D., Liu, B., Zhang, W., et al. (2018). The Role of the Solid Electrolyte Interphase Layer in Preventing Li Dendrite Growth in Solid-State Batteries. *Energy Environ. Sci.* 11, 1803–1810. doi:10.1039/c8ee00540k

Xia, S., Wu, X., Zhang, Z., Cui, Y., and Liu, W. (2019). Practical Challenges and Future Perspectives of All-Solid-State Lithium-Metal Batteries. *Chem* 5, 753–785. doi:10.1016/j.chempr.2018.11.013

Yang, T., Zheng, J., Cheng, Q., Hu, Y.-Y., and Chan, C. K. (2017). Composite Polymer Electrolytes with Li7La3Zr2O12 Garnet-type Nanowires as Ceramic Fillers: Mechanism of Conductivity Enhancement and Role of Doping and Morphology. *ACS Appl. Mater. Inter.* 9, 21773–21780. doi:10.1021/acsami.7b03806

Yang, X., Sun, Q., Zhao, C., Gao, X., Adair, K. R., Liu, Y., et al. (2019). High-Areal-Capacity All-Solid-State Lithium Batteries Enabled by Rational Design of Fast Ion Transport Channels in Vertically-Aligned Composite Polymer Electrodes. *Nano Energy* 61, 567–575. doi:10.1016/j.nanoen.2019.05.002

Yue, L., Ma, J., Zhang, J., Zhao, J., Dong, S., Liu, Z., et al. (2016). All Solid-State Polymer Electrolytes for High-Performance Lithium Ion Batteries. *Energ. Storage Mater.* 5, 139–164. doi:10.1016/j.ensm.2016.07.003

Zeng, H., Ji, X., Tsai, F., Zhang, Q., Jiang, T., Li, R. K. Y., et al. (2018). Enhanced Cycling Performance for All-Solid-State Lithium Ion Battery with LiFePO4 Composite Cathode Encapsulated by Poly (Ethylene Glycol) (PEG) Based Polymer Electrolyte. *Solid State Ionics* 320, 92–99. doi:10.1016/j.ssi.2018.02.040

Zhang, W., Nie, J., Li, F., Wang, Z. L., and Sun, C. (2018). A Durable and Safe Solid-State Lithium Battery with A Hybrid Electrolyte Membrane. *Nano Energy* 45, 413–419. doi:10.1016/j.nanoen.2018.01.028

Zhang, X., Wang, S., Xue, C., Xin, C., Lin, Y., Shen, Y., et al. (2019). Self-Suppression of Lithium Dendrite in All-Solid-State Lithium Metal Batteries with Poly(vinylidene difluoride)-Based Solid Electrolytes. *Adv. Mater.* 31, 1806082. doi:10.1002/adma.201806082

Zhou, W., Wang, Z., Pu, Y., Li, Y., Xin, S., Li, X., et al. (2019). Double-Layer Polymer Electrolyte for High-Voltage All-Solid-State Rechargeable Batteries. *Adv. Mater.* 31, 1805574. doi:10.1002/adma.201805574

Zhu, P., Yan, C., Dirican, M., Zhu, J., Zang, J., Selvan, R. K., et al. (2018). Li0.33La0.557TiO3 Ceramic Nanofiber-Enhanced Polyethylene Oxide-Based Composite Polymer Electrolytes for All-Solid-State Lithium Batteries. *J. Mater. Chem. A.* 6, 4279–4285. doi:10.1039/c7ta10517g

Zou, P., Wang, Y., Chiang, S.-W., Wang, X., Kang, F., and Yang, C. (2018). Directing Lateral Growth of Lithium Dendrites in Micro-Compartmented Anode Arrays for Safe Lithium Metal Batteries. *Nat. Commun.* 9, 464. doi:10.1038/s41467-018-02888-8

Conflict of Interest: The authors declare that the research was conducted in the absence of any commercial or financial relationships that could be construed as a potential conflict of interest.

Publisher's Note: All claims expressed in this article are solely those of the authors and do not necessarily represent those of their affiliated organizations, or those of the publisher, the editors, and the reviewers. Any product that may be evaluated in this article, or claim that may be made by its manufacturer, is not guaranteed or endorsed by the publisher.